DESIGN OPTIMIZATION OF A NOVEL MAGNETIC SWITCHABLE DEVICE BASED ON HALBACH ARRAY

Yong Chen[*], Changming Wang, and Jiandong Bao

Nanjing University of Science and Technology, Nanjing, China

Abstract—The paper deals with the design and optimization of a novel magnetic switchable device based on Halbach array. The magnetic field in air gap is adjustable by rotating the center axis of adhesion mechanism so that the magnetic adhesion force is variable, and it is convenient for device to adsorb on and detach from the ferromagnetic workpiece or surface. The magnetic field model is established by Fourier series method, and the optimal dimensions of configuration are obtained by genetic algorithms for best performing design. The magnetic force of novel optimal device is measured, and a good agreement between simulation and measurement is found. The results are compared to the traditional mechanism, and it is shown that the utilization ratio of magnets of novel optimal mechanism is 2.2 times larger than the H-type one with the same usage of magnets, while its consumption of soft iron is only 12.7% of the H-type one.

1. INTRODUCTION

Coils, electromagnets or permanent magnets have been used extensively as attachment mechanism [1]. The electromagnetic forces produced by coils and electromagnets strongly depend on energizing coil ampere turns, thus inevitably causing problems, such as high power consumption, high temperature, potential safety hazard, short service life, heavy weight, high maintenance cost. Permanent magnetic adhesion mechanism (PMAM) is highly desirable due to its inherent reliability and spending no extra energy for adhesion process. Especially, in the case of a total loss of the power supplied, with PMAM, it will not cause the problem of magnetic force suddenly disappearing compared with electromagnets. Examples of applications

where a PMAM can be used are magnetic pad and footprint shape for human climbing [2], holding device [3] and wall-climbing robot [4].

The defect of PMAM does not change magnetic field easily compared with the electromagnetic adhesion mechanism. The magnetic field of permanent magnet in free space is invariable without any mechanical operation in general condition. An energy efficient solution is to use Magnetic Switchable Device (MSD) [1]. The configuration has been widely used as holding device for decades and recently is applied to wall-climbing robots [5–7] and motors [8–11]. The PMAM with a switchable pole, like H-type, is used in wheel-type wall-climbing robot [6]. The robot can operate up and down on the ferromagnetic wall easily by changing the orientation of the magnetic pole. However, the consumption of iron yoke in the H-type configuration is so much that payload capacity of robot is decreased. In addition, the low utilization ratio of permanent magnet and continuously increasing price of rare earth material obstruct the application of MSD.

In this paper, a novel magnetic switchable adhesion device is designed, and its magnetic field model is established by Fourier series method. The optimal dimensions of the mechanism will be also investigated in genetic algorithms. Then the resulting design is dimensioned and then characterized by comparing magnetic force measurements to the traditional H-type MSD design.

2. MODELING THE NOVEL MSD

2.1. Basic Topologies of MSD

It is noted that the magnetic circuit design significantly affects the performance of MSD, such as adhesion reliability, detachment flexibility, payload capacity and operation efficiency. However, integration of these performance parameters is still an essential issue demanding a promote solution. In order to solve this problem, a novel design of MSD based on linear Halbach array is proposed for detailed investigation. Here the novel design that differs from existing configurations has three combined characteristics such as new magnetization arrangement of permanent magnets for high utilization of magnetic materials, lower usage of soft iron and convenient switchable magnetic force. However, the traditional MSD only has one or two of them. For example, H-type MSD [6] has conveniently switchable magnetic force but large consumption of iron and low utilization of magnets due to the single magnetization arrangement. And the design in [5] has advantage of less usage of iron but hard to make the adhesion force switchable.

Halbach magnet arrays are new magnetization arrangement of permanent magnets, which were used by Klauss Halbach for particle accelerators [12], and they have slowly migrated into the arena of electromechanics. These magnet arrays have been suggested as the field source of choice for linear permanent magnet machines [13], synchronous machines [14] and high speed magnetically levitated vehicles (Maglev) [15]. Ideal linear Halbach array has pure sine- and cosine-magnetic profiles in the horizontal and vertical directions, respectively, on the enhanced side of the array, while cancelling the field on the other side. Its magnetization direction continuously changes along the array, but it is impractical to fabricate. Instead, an array of segmented rectangular or square permanent magnets is actually used, each of which has a direction of magnetization equal to the direction of magnetization of a continuous linear Halbach array at the center of the segment [16]. Consequently, there are problems of non-zero flux on the cancelled side and ends effect existing in the segmented linear Halbach array so that it cannot be directly used as a MSD. Taking these points into account, a novel configuration of MSD is obtained.

The three-dimensional prototype of the device is composed of 5-segmented linear Halbach array, soft iron and rotating axis, which is shown in Fig. 1. In the figure, the coordinates o-xyz is used; arrows are the direction of the remanent magnetization of the magnetic material; a and b are the lengths of vertical and horizontal magnetization magnets, respectively; d is the height of the magnets; h_1 and h_2 are the thicknesses of end sides of the array and soft iron on upper, respectively; c is the width of magnets and soft iron. The magnetization direction of magnets is arranged as Fig. 1 so that the enhanced side of array is on the bottom of the mechanism as main adhesion surface. The additive soft iron is fixed on the upper side and end sides of the array so that it could resolve the problems of non-zero flux in cancelled side and ends effect. The rotating axis is driven by
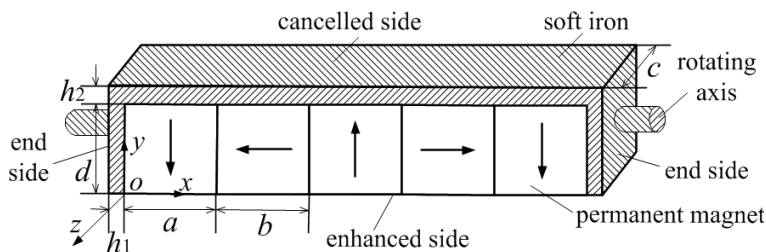
Figure 1. A sketch of novel magnetic adhesion mechanism.

motor so that it can make the flux density in air gap switchable.

2.2. Analysis of Magnetic Field and Adhesion Force

In order to analyze the performance of the novel MSD, its magnetic field distribution and adhesion force are investigated. The ideal linear Halbach array has an infinite size in space, and its magnetization vectors are changed smoothly and continuously according to sinusoid variation. For an ideal Halbach array, the magnetizations are given by:

$$\mathbf{M} = m_x\mathbf{i} + m_y\mathbf{j} = \sum_{n=-\infty}^{\infty}(m_{xn}\mathbf{i} + m_{yn}\mathbf{j})$$

$$= \sum_{n=-\infty}^{\infty}m_{n0}[\mathbf{i}\sin(k_nx) + \mathbf{j}\cos(k_nx)] \tag{1}$$

where m_{xn} and m_{yn} are the horizontal and vertical magnetizations. $k_n = 2\pi n/\lambda$ is the spatial wave number of the nth harmonic and m_{n0} the peak value of magnetization.

According to the scale magnetic potential method [17], for permanent magnet sheet, the magnetic scalar potential φ within the sheet obey Poisson's equation:

$$\nabla^2\varphi = \nabla \cdot \mathbf{M} = m_{n0}k_n\cos(k_nx) \tag{2}$$

and Laplace's equation outside of the sheet:

$$\nabla^2\varphi = 0 \tag{3}$$

Equations (2) and (3) can be solved using the boundary conditions. The potentials are continued at the boundary and go to zero at infinity. The flux density of the normal component is also continuous. The potentials of cancelled and enhanced sides, φ_1 and φ_2 are given by:

$$\begin{cases} \varphi_1 = 0 \\ \varphi_2 = \sum_{n=-\infty}^{\infty}\dfrac{m_{n0}}{k_n}\left(1 - e^{k_nd}\right)e^{k_ny}\cos(k_nx) \end{cases} \tag{4}$$

and the magnetic fields are given by:

$$\begin{cases} \mathbf{H}_1 = 0 \\ \mathbf{H}_2 = -\left(\mathbf{i}\dfrac{\partial}{\partial x} + \mathbf{j}\dfrac{\partial}{\partial y}\right)\varphi = \sum_{n=-\infty}^{\infty}m_{n0}\left[-\mathbf{i}\left(1 - e^{k_nd}\right)e^{k_ny}\sin(k_nx)\right. \\ \left. \qquad -\mathbf{j}\left(1 - e^{k_nd}\right)e^{k_ny}\cos(k_nx)\right] \end{cases} \tag{5}$$

However, the practical Halbach array cannot make the magnetization vectors change smoothly and continuously in real applications. It often uses segmented magnet cubes combining together for substitute. Using the Fourier series method and combining with the Eq. (5), the magnetic field of practical Halbach array is given:

$$
\begin{cases}
\mathbf{H}_1 = \sum_{n=3,7\ldots(4i-1)}^{\infty} m_0 \left[\mathbf{i} A_n \left(1 - e^{nk_1 d} \right) e^{nk_1|y|} \sin(nk_1 x) \right. \\
\qquad \left. + \mathbf{j} A_n \left(1 - e^{nk_1 d} \right) e^{nk_1|y|} \cos(nk_1 x) \right] \\
\mathbf{H}_2 = \sum_{n=1,5\ldots(4i+1)}^{\infty} m_0 \left[\mathbf{i} A_n \left(1 - e^{nk_1 d} \right) e^{nk_1|y|} \sin(nk_1 x) \right. \\
\qquad \left. + \mathbf{j} A_n \left(1 - e^{nk_1 d} \right) e^{nk_1|y|} \cos(nk_1 x) \right]
\end{cases}
\tag{6}
$$

where $A_n = -\frac{4}{n\pi} \left[\sin\left(\frac{\pi n}{2}\right) \cos(\pi n) \sin\left(\frac{\pi n b}{2(a+b)}\right) \right]$ is the Fourier series, $k_1 = 2\pi/[\nu(a+b)]$ the wave number, and ν the numbers of magnets per wavelength. The configuration parameters are originally used for analysis with 8 mm length of magnet cube, $h_1 = h_2 = 3$ mm, air gap length $\delta = 1$ mm. The value of magnetic field distribution of the mechanism in air gap in operating and non-operating state, i.e., $B_{\max}$ and $B_{\min}$, is calculated and shown in Fig. 2. It is seen from Fig. 2 that the magnetic field value of the mechanism in operating state is very strong, especially in vertical component of magnetic field, $B_{\max y}(x)$,
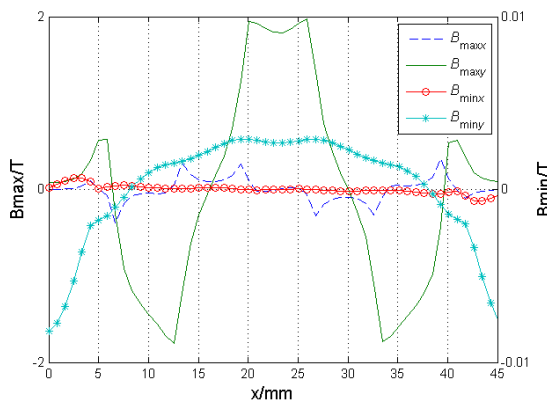
Figure 2. Air gap magnetic field distribution of the mechanism for $\delta = 1$ mm.

which is the main source of the adhesion force. On the contrary, also in Fig. 2, the magnetic field in non-operating state is very weak and close to zero.

In addition, two-dimensional analysis of magnetic flux line of the two states is performed using a commercial FEM tool, ANSYS software, and is shown in Fig. 3. As can be seen in Fig. 3(a), there is little magnetic leakage flux out of the soft iron, and the magnetic flux density is gathered in the air gap on the ends of the device, which improves the adhesion force. Moreover, the flux in air gap is homogeneous so that the adaptive capability on ferromagnetic surface is enhanced, and flux in soft iron is dense so that the fixing of magnets of array becomes easy. In Fig. 3(b) the flux lines of the device in the air gap approach zero as they form loops through the soft iron, which helps the device detach from workpiece and surface conveniently.

(a) operating state

(b) non-operating state
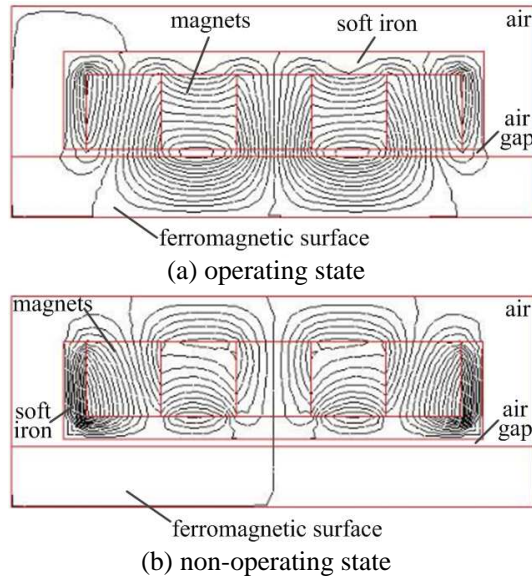
Figure 3. Two-dimensional magnetic flux maps of two states.

Furthermore, the adhesion force of two states of the mechanism with and without soft iron is calculated by Maxwell stress tensor method [18]. The results are: $F_{\max 1} = 277.0\,\text{N}$, $F_{\max 2} = 238.0\,\text{N}$, $F_{\min 1} = 0.04\,\text{N}$ and $F_{\min 2} = 44.5\,\text{N}$, where $F_{\max}$, $F_{\min}$ is the magnetic adhesive force produced by mechanism in operating and non-operating state, and subscripts 1, 2 mean with and without iron, respectively. The calculations indicate that the mechanism with soft iron could

produce larger $F_{\max}$ and smaller $F_{\min}$ than it is without soft iron which can meet the requirements of design. The almost zero value $F_{\min 1}$ makes the MSD detach from the ferromagnetic surface conveniently.

It is not sufficient to characterize a design only by the value of field flux density and magnetic force. The utilization ratio of magnets and consumption of the magnetic materials and soft iron should also be considered. Therefore, in the next section the optimization of the magnetic adhesion mechanism for best performance is investigated.

3. OPTIMIZATION OF MSD

3.1. Design Variables

By the analysis above, it can be seen that there are mainly six design variables of MSD, including a, b, d, c, h_1 and h_2. To simplify the optimal design of the MSD, some of the design variables above are determined in advance according to analysis. It is obvious that the value of adhesion area in air gap and the weight of device are both increased with increasing width of device. In this paper, the width of device c is fixed at $0.008\,\mathrm{m}$ for the convenience of discussion, and the force per width is used for optimization. For a PMAM with a constant size, it was found that if the thickness of soft iron is too thin, it will lead to magnetic saturation and thus reduce the magnetic force; if it is too thick, it will offer redundant paths for the magnetic flux of the permanent magnet and increase the volume of the magnetic adhesion device. The thickness h_1 mainly improves air gap flux density of two ends of array on enhanced side, and the thickness h_2 mainly reduces the magnetic leakage on cancelled side. Therefore, the proper values of $h_1 = 0.004\,\mathrm{m}$ and $h_2 = 0.001\,\mathrm{m}$ are suggested in this paper in order to decrease the weight of PMAM, to improve the magnetic field on ends of array, to avoid magnetic saturation as far as possible, and also to reduce the number of design variables and thus simplify the optimization design of the PMAM.

Consequently, the number of design variables becomes three which comprise the vector $\mathbf{x} = [a\ b\ d]$. By combining their physical meanings and the present level of mechanical machining techniques, their ranges are determined and described as (unit: m): $a, b, d \in [4, 15] \times 10^{-3}$.

3.2. Constrains

We define $\bar{F}_{\max}(\mathbf{x})$, $\bar{F}_{\min}(\mathbf{x})$ and $V_m(\mathbf{x})$ as the procedure variables of $\bar{F}_{\max}$, $\bar{F}_{\min}$ and V_m with design variable vector $\mathbf{x}$, where $\bar{F}_{\max}$ and $\bar{F}_{\min}$ are maximal and minimal adhesion forces per unit length respectively, and V_m is the volume of magnets. In order to improve the adhesion

reliability and release flexibility, $\bar{F}_{\max}(\mathbf{x})$ should be larger than the original value $\bar{F}_{\max 0}$, and $\bar{F}_{\min}(\mathbf{x})$ should be smaller than the original value $\bar{F}_{\min 0}$, which are both in the same consumption of magnetic materials, i.e., $V_m(\mathbf{x})$ is equal to the original value V_{m0}. Therefore, the design constrains are summarized and expressed as:

$$\left\{ \begin{array}{l} h(\mathbf{x}) = 0 \\ g_1(\mathbf{x}) \leq 0, \ g_2(\mathbf{x}) \leq 0 \end{array} \right. \tag{7}$$

where $h(\mathbf{x}) = V_m(\mathbf{x}) - V_{m0}$, $g_1(\mathbf{x}) = \bar{F}_{\max 0} - \bar{F}_{\max}(\mathbf{x})$, $g_2(\mathbf{x}) = \bar{F}_{\min}(\mathbf{x}) - \bar{F}_{\min 0}$.

3.3. Objective Function

As mentioned above, the design target is to improve the utilization of permanent materials, i.e., maximal magnetic force per unit volume, and the ratio of maximum to minimum magnetic force. Therefore, the objective function is:

$$\left\{ \begin{array}{l} \min f_1(\mathbf{x}) = \dfrac{V_m(\mathbf{x})}{F_{\max}(\mathbf{x})} = \dfrac{(n_a a + n_b b)d}{\bar{F}_{\max}(\mathbf{x})} \\ \min f_2(\mathbf{x}) = \dfrac{F_{\min}(\mathbf{x})}{F_{\max}(\mathbf{x})} = \dfrac{\bar{F}_{\min}(\mathbf{x})}{\bar{F}_{\max}(\mathbf{x})} \end{array} \right. \tag{8}$$

where n_a, n_b is the numbers of vertical and horizontal magnetization magnets, respectively.

It is obvious that Eq. (8) is a multi-objective optimization function. In order to solve this problem, we convert it to a single objective function by using the linear weighting method. The sub-objective functions of $f_1(\mathbf{x})$ and $f_2(\mathbf{x})$ are optimized respectively, and the corresponding optimal solutions are f_1^* and f_2^*. Then commonly using their reciprocal as weight coefficient, i.e., $\omega_i = 1/f_i^* \geq 0$, the integrated single objective function can be expressed as:

$$\min f(\mathbf{x}) = \sum_{i=1}^{2} \omega_i f_i(\mathbf{x}) \tag{9}$$

Moreover, it is noted that the value of $f_1(\mathbf{x})$ is much less than $f_2(\mathbf{x})$. In order to use Eq. (9) to solve the optimization problem with a single objective function conveniently, the transformation formulas are defined as:

$$f_1'(\mathbf{x}) = 10^M f_1(\mathbf{x}) \tag{10}$$

$$M = [\lg(f_2(\mathbf{x}))] - [\lg(f_1(\mathbf{x}))] \tag{11}$$

where lg is common logarithm, and [ ] is Gauss integer function.

By Eqs. (10) and (11), the values of $f_1'(\mathbf{x})$ and $f_2(\mathbf{x})$ become the same order of magnitude, and the important degree of objective

function denoted by weight coefficient ω_i also becomes the same order of magnitude. Then the weight coefficient ω_i can be normalized to Eq. (12):

$$\begin{cases} \omega_1 = \dfrac{1/f_1^{'*}(x)}{1/f_1^{'*}(x) + 1/f_2^*(x)} \\ \omega_2 = \dfrac{1/f_2^*(x)}{1/f_1^{'*}(x) + 1/f_2^*(x)} \end{cases} \tag{12}$$

3.4. Solution and Results

Multi-parameter, multi-peak value and nonlinear optimal problem, and the globally optimal solution cannot be easily obtained by traditional optimization algorithm. In this paper, the genetic algorithm (GA) is used for its strong robustness and validity to solve the problem [19]. Genetic algorithms are search procedures whose mechanics are based on those of natural genetics, which can find multiple globally optimal solutions directly and efficiently in a single run. Thus GA is selected to solve the problem, and fitness function should be determined at first. Fitness function is a criterion used to evaluate the adaptation quality of individuals in population and is obtained by construction method of boundary:

$$F(\mathbf{x}) = \begin{cases} \varepsilon_{\max} - f(\mathbf{x}), & f(\mathbf{x}) < \varepsilon_{\max} \\ 0, & f(\mathbf{x}) \geq \varepsilon_{\max} \end{cases} \tag{13}$$

where $\varepsilon_{\max}$ is the current maximum of objective function of all generations. As GA cannot directly deal with the optimization problem with constraint condition, it has to be transformed into unconstrained optimization problem. Considering the constraint condition in Eq. (13), the penalty function is constructed as follows [20]:

$$\begin{cases} \upsilon(\mathbf{x}) = r^{(\tau)} \displaystyle\sum_{i=1}^{2} g_i(\mathbf{x}) \\ \mu(\mathbf{x}) = \dfrac{1}{\sqrt{r^{(\tau)}}} h^2(\mathbf{x}) \end{cases} \tag{14}$$

where $r^{(\tau)}$ is penalty factor. Let $r^{(\tau)} \to 0$ and initial value $r^{(0)} = 0$. τ is the current number of genetic generation.

The basic genetic algorithm is composed of four main stages, i.e., initialization, selection, crossover and mutation.

Firstly, an initial population is generated randomly or in some cases based on expert data. The fitness of each individual in this population is examined through an optimization objective function.

Secondly, a selection method is applied to the initial population to choose the parents. Several methods have been proposed for selection. In this paper, the Roulette Wheel method is used. The genetic operators are then applied to the parents to generate a new population. Elitist rules are also employed to prevent missing elite individuals in each population.

Thirdly, the crossover operator combines the features of two parent chromosomes to create new solutions. In this paper, the cross probability is calculated according to formula (15). Both the parent and offspring populations will be reserved in the current population.

$$P_c = \begin{cases} P_{c1} - \frac{P_{c1} - P_{c2}}{f_{\max} - f_{avg}} \left(f' - f_{avg} \right), & \text{when } f' \geq f_{avg} \\ P_{c1}, & \text{when } f' < f_{avg} \end{cases} \tag{15}$$

where $f_{\max}$ denotes the maximal fitness of current population, f_{avg} the average fitness of each generation, f' the larger fitness of two parent chromosomes which need to crossover, anf P_{c1} and P_{c2} denote the maximal and minimal cross probability respectively.

Finally, mutation takes place on some newly formed children in order to prevent all solutions from converging to their particular local optima. As you know, using one certain mutation operator may not solve the given optimization problem perfectly and will reduce the effectiveness and efficiency of GA. So we try to select the adaptive mutation operators to execute the genetic evolution according to the performance of these mutation operators. In this paper, the mutation probability of each individual is calculated according to formula (16).

$$P_m = \begin{cases} P_{m1} - \frac{P_{m1} - P_{m2}}{f_{\max} - f_{avg}} (f_{\max} - f), & \text{when } f \geq f_{avg} \\ P_{m1}, & \text{when } f < f_{avg} \end{cases} \tag{16}$$

where f denotes the fitness of individual which need to mutation, and P_{m1} and P_{m2} denote the maximal and minimal mutation probability respectively.

This procedure is repeated until optimal parameter values are achieved. The GA parameters used in this paper are listed in Table 1.

The optimal solution is obtained combining Eqs. (7)–(16), which is shown in Table 2. It is seen that the values of $\bar{F}_{\max}$ and $\bar{F}_{\min}$ are better than the original parameters with the low consumption of magnets which means the larger value of η. Here η is the utilization ratio of magnets defined as [15]:

$$\eta = \frac{F_{\max}}{V_m} = \frac{\bar{F}_{\max}}{(n_a a + n_b b)d} \tag{17}$$

It can be seen from Table 2 that the increment of η is about 6.2%.

Table 1. Genetic algorithm parameters.

Parameters	Description	Value
N_{pop}	Size of population	100
N_{gen}	Number of generations	1000
N_{pre}	Number of pretenders (in elitist strategy)	3
P_{c1}	Maximal cross probability	0.9
P_{c2}	Minimal cross probability	0.6
P_{m1}	Maximal mutation probability	0.1
P_{m2}	Minimal mutation probability	0.001

Table 2. Parameters optimization solution list.

	a (m)	b (m)	d (m)	$\bar{F}_{\max}$ (N/m)
Original	0.008	0.008	0.008	34622.5
Optimal	0.0105	0.0055	0.0075	36610.8
	$\bar{F}_{\min}$ (N/m)	V_m (m³)	f_1 (m³/N)	f_2
Original	5.0	2.56×10^{-6}	9.24×10^{-9}	1.44×10^{-4}
Optimal	3.6	2.55×10^{-6}	8.71×10^{-9}	9.83×10^{-5}

4. COMPARISON AND EXPERIMENTAL TEST

4.1. Compared with H-type Mechanism

To find excellent performance of the novel optimal configuration, we have chosen to show a comparison between H-type and novel mechanism. The prototype of the novel magnetic switchable device has been built based on above optimal dimension parameters (see Table 2). The optimal dimension parameters of the H-type configuration (see Fig. 4) are selected from [6]: width of mechanism, $A = 90$ mm, radius of cylinder, $R = 22$ mm, width of magnetic insulation material, $D = 11$ mm, height of soft iron, $G = 65$ mm. In order to compare with each other in the same size, the length of mechanism, l, is selected for 42 mm, and the other optimal parameters of H-type configuration are reduced in scaling of 5 times smaller than the original one, i.e., $A' = 18$ mm, $R' = 4.4$ mm, $D' = 2.2$ mm, $G' = 13$ mm. The magnetic materials parameter of H-type is used same as this paper. The performance comparison of the two types of mechanism is given
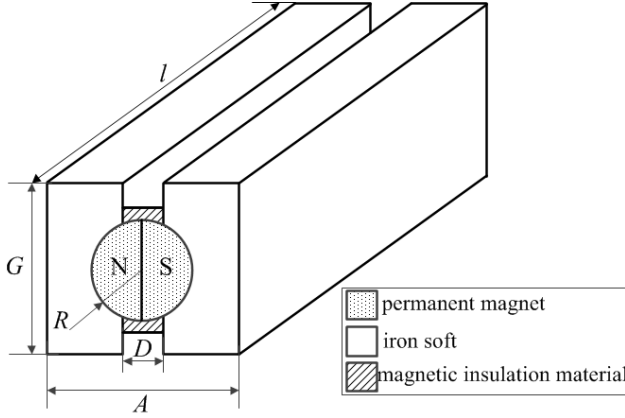
Figure 4. A sketch of H-type magnetic adhesion mechanism.

Table 3. Parameters comparison between two types of mechanism with $\delta = 0.001$ m.

Parameters	H-type one	Novel optimal one
$F_{\max}$ (N)	132.83	292.89
$F_{\min}$ (N)	0.06	0.028
V_m (m^3)	2.554×10^{-6}	2.55×10^{-6}
η (N/m^3)	5.2×10^7	1.15×10^8
V_s (m^3)	6.876×10^{-6}	0.870×10^{-6}

where the volume of soft iron is V_s.

in Table 3. It is seen that the values $F_{\max}$ and η of novel optimal mechanism are 2.2 times larger than the H-type one with the same usage of magnets, while its consumption of soft iron is only 12.7% of the H-type one.

4.2. Experimental Test

Experiment was set up to test the numerical optimization results. The maximum and minimum adhesion forces of novel original, novel optimal and H-type magnetic switchable device were tested by using lifting weight method. The device was adsorbed on the horizontal ferromagnetic surface which was fixed on the ground, and the air gap length can be adjusted by the adjusting screw. The forces were

measured by the resistance strain sensor for the air gap length at every other millimeter during the range of $1 \sim 11\,\text{mm}$. One end of the sensor was connected with the center body of the adhesion mechanism, and the weight hung at the other end through the fixed pulley. By increasing the weight continuously, the adhesion forces can be measured when the device was just detached from the surface.

The comparison of $F_{\max}$, $F_{\min}$ in numerical simulation and measurement data is shown in Fig. 5, and a good agreement between them is seen. The small error between the measured data and the simulation results is caused by several factors. The size of real model is influenced by machining precision, and there is space between magnets for neoprene adhesive by each other. In addition, we use stepper motor to drive the adhesion mechanism to change the air gap length, which cannot ensure all the measurement points in the state that the adhesion area of mechanism is parallel to ferromagnetic plane. The comparison of adhesion force between H-type and the novel device is also shown in Fig. 5, and it is obvious that the performance of novel one is better than the H-type one. In addition, the performance of novel optimal design is better than the original design.
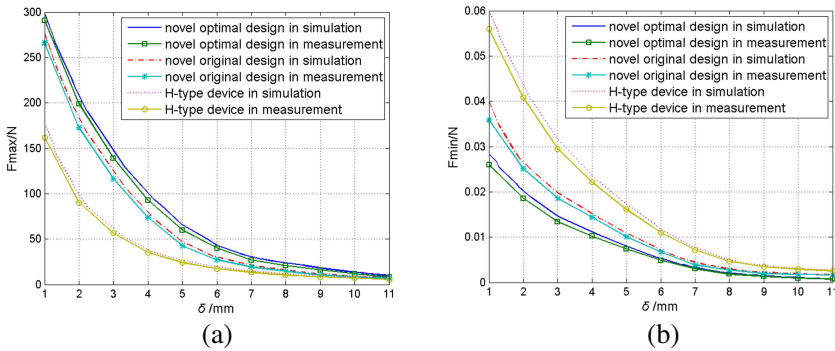
Figure 5. Comparison of adhesion force between simulation and measurement, the original and optimal, H-type and the novel.

We can further get the good qualities of the novel MSD from comparison as follows:

1) The larger utilization ratio of permanent magnet materials. Looking at Table 3, with less usage of magnet materials, the novel configuration has a much larger value of η than the H-type one. So it can produce much greater maximal adhesion force with the same volume of magnet and save a lot of permanent magnet materials for meeting the requirement of $F_{\max}$.

2) The stronger adhesion ability and detachable flexibility. As can be seen from Table 3, the novel mechanism is able to produce larger maximal adhesion force in operating state and smaller minimal adhesion force in non-operating state, which means the mechanism adhering to workpiece or surface reliably and detaching from it conveniently.

3) The greater payload capacity. It is important to found from the results that the new adhesion mechanism saves a large amount of consumption of materials, not only permanent magnets but also soft iron compared with the H-type one. It uses only a little soft iron to improve the magnetic field on cancelled side and end sides. So by reducing the weight of itself, its payload ability is improved, which is important for adhesion mechanisms.

4) The better adaptive capability on surface. The larger F_{max} with δ varied from 1 mm to 11 mm in Fig. 5 shows that the novel mechanism could have better capability to be adapted on concave and convex ferromagnetic surface. Therefore, it can be used in much worse situation, which will enlarge its application field.

5. CONCLUSION

The design and optimization of a newly magnetic switchable device was presented. The one side flux density characteristic of Halbach array was used to produce operating and non-operating state, i.e., adhesion and detachment on surface. The rotating axis was driven by motor so that it can make the flux density in air gap switchable. A little additive soft iron was used to resolve the problem of non-zero flux density on cancelled side and magnetic leakage on end sides of a practical array. The magnetic field of ideal and practical array is modeled by scale magnetic potential method and Fourier series method respectively. The optimal dimensions of the mechanism were obtained with the greatest utilization ratio of magnetic materials. The novel optimal configuration was compared to the traditional adhesion mechanism and was 2.2 times larger than the H-type one with the same usage of magnets, while its consumption of soft iron is only 12.7% of the H-type one. Finally, the results were proved by the comparison of magnetic force in simulation and measurement.

ACKNOWLEDGMENT

REFERENCES

1. Rochat, F., S. Patrick, B. Michael, M. Stephane, M. Francesco, and B. Hannes, "Design of magnetic switchable device (MSD) and applications in climbing robot," *Proc. of 13th Int. Conference on Climbing and Walking Robots and the Support Technologies for Mobile Machines*, 357–382, 2010.

2. Jose, B., T. Kenjiro, K. Tatsuaki, and K. Robert, "Compliant distributed magnetic adhesion device for wall climbing," *Proc. of the IEEE Int. Conference on Robotics and Automation*, 10–14, Roma, 2007.

3. Coey, J. M. D., "Permanent magnet applications," *J. Magn. Magn. Mater.*, Vol. 248, 441–456, 2002.

4. Chu, B., K. Jung, C. S. Han, J. Kim, and D. Hong, "A survey of climbing robots: Locomotion and adhesion," *Int. J. Precis. Eng. Manuf.*, Vol. 11, No. 4, 633–647, 2010.

5. Fischer, W., F. Tache, and R. Siegwart, "Magnetic wall climbing robot for thin surfaces with specific obstacles," *Field and Service Robotics*, Vol. 42, 551–561, 2008.

6. Yao, P. X. and D. W. Li, "The magnetic field analysis and optimization of permanent-magnetic adhesion device for a novel wall-climbing robot," *Proc. of the IEEE Conference on International Technology and Innovation*, 2–6, 2009.

7. Zhang, Y. M., T. Dodd, K. Atallah, and I. Lyne, "Design and optimization of magnetic wheel for wall and ceiling climbing robot," *Proc. of the IEEE Int. Conference on Mechatronics and Automation*, 1393–1398, 2010.

8. Zhao, W., M. Cheng, R. Cao, and J. Ji, "Experimental comparison of remedial single-channel operations for redundant flux-switching permanent-magnet motor drive," *Progress In Electromagnetics Research*, Vol. 123, 189–204, 2012.

9. Liu, C. and K.-T. Chau, "Electromagnetic design and analysis of double-rotor flux-modulated permanent-magnet machines," *Progress In Electromagnetics Research*, Vol. 131, 81–97, 2012.

10. Torkaman, H. and E. Afjei, "Comparison of three novel types of two-phase switched reluctance motors using finite element method," *Progress In Electromagnetics Research*, Vol. 125, 151–164, 2012.

11. Torkaman, H. and E. Afjei, "Magnetostatic field analysis regarding the effects of dynamic eccentricity in switched reluctance motor," *Progress In Electromagnetics Research M*, Vol. 8, 163–180, 2009.

12. Halbach, K., "Design of permanent multipole magnets with oriented rare Earth cobalt material," *Nucl. Instrum. Methods*, Vol. 169, 1–10, 1981.

13. Liang, Y., L. Zhang, T. Wang, Z. Jiao, C.-Y. Chen, and I.-M. Chen, "Magnetic field of tubular linear machines with dual Halbach array," *Progress In Electromagnetics Research*, Vol. 136, 283–299, 2013.

14. Jang, S. and L. Sung, "Comparison of two types of PM linear synchronous servo and miniature motor with air cored film coil," *IEEE Trans. Magn.*, Vol. 38, No. 5, 3264–3266, 2002.

15. Guo, F., Y. Tang, L. Ren, and J. Li, "Structural parameter optimization design for Halbach permanent maglev rail," *Physica C: Superconductivity*, Vol. 470, No. 20, 1787–1790, 2010.

16. Choi, J. S. and J. Yoo, "Design of a Halbach magnet array based on optimization techniques," *IEEE Trans. Magn.*, Vol. 44, No. 10, 2361–2366, 2008.

17. Shute, H. A., J. C. Mallinson, D. T. Wilton, and D. J. Mapps, "One-sided fluxes in planar, cylindrical, and spherical magnetized structures," *IEEE Trans. Magn.,* Vol. 36, No. 2, 440–451, 2000.

18. Mahmoudi, A., N. A. Rahim, and H. W. Ping, "Axial-flux permanent-magnet motor design for electric vehicle direct drive using sizing equation and finite element analysis," *Progress In Electromagnetics Research,* Vol. 122, 467–496, 2012.

19. Seok, O. and S. L. Jin, "Hybrid genetic algorithms for feature selection," *IEEE Transactions on Pattern Analysis and Machine Intelligence*, Vol. 26, No. 11, 1424–1437, 2004.

20. Bai, Z. C. and X. N. Li, "Optimization design of magnetorheological damper inserted into servo pneumatic rotary actuator," *Journal of Nanjing University of Science and Technology*, Vol. 36, No. 3, 534–539, 2012.